Geomorphology 261 (2016) 212–221

Contents lists available at ScienceDirect

Geomorphology

journal homepage: www.elsevier.com/locate/geomorph

# Seepage weathering impacts on erosivity of arid stream banks: A new conceptual model

Uri Nachshon

*Institute of Soil, Water and Environmental Sciences, Agricultural Research Organization, The Volcani Research Center, Bet-Dagan 50250, Israel*

ARTICLE INFO

*Article history:*
Received 20 September 2015
Received in revised form 9 March 2016
Accepted 10 March 2016
Available online 12 March 2016

*Keywords:*
Seepage erosion
Salt weathering
Pipe erosion
Solute
Transport

ABSTRACT

Field observations have indicated the formation of horizontal, pipe shape cavities, along gully and dry stream channel banks in the semi-arid region of the northern Negev Desert, Israel. Piping is a well-known phenomenon in humid regions due to subsurface water flow and seepage weathering. However, in dry environments where rain events are scarce and subsurface water flow is rare, it is proposed here that capillary flow of saline water in the vadose zone leads to similar processes. It is suggested that where saline and shallow ground water persists, capillary flow may result in salt accumulation and precipitation at the top of the capillary fringe, consequently rendering this zone to be more susceptible to erosion. A conceptual model is presented and field observations, laboratory experiments, and a physically-based model are used to prove the feasibility of the proposed conceptual model and to explain why salts accumulate at the top of the capillary fringe, even though evaporation acts all along the vertical stream channel or gully banks. It is suggested that the low evaporative flux, in comparison to the liquid water flux, disables salt accumulation along the profile to the top of the capillary fringe where the liquid water flux is minimal. The presented findings strengthen the conceptual model, but thorough field studies are needed to estimate the impact of the proposed mechanism on erosion processes on a field scale.



## 1. Introduction

Soil erosion is considered to be the major cause of soil degradation worldwide, and it is estimated that more than 1000 and 500 million ha of land have been deteriorated worldwide by water and wind erosion, respectively (Lal, 2003). Recently, several studies have explored the impact of subsurface hydro-geochemical processes on soil erosion and it was shown that the location of solutes accumulation within the soil profile is a key element affecting the formation of pipes, tunnels, and cavities along slopes and stream channel banks (e.g., Faulkner, 2006; Lamb et al., 2006, 2007, 2008; Fox et al., 2007a; Fox and Wilson, 2010; Wilson et al., 2012, 2015). Faulkner et al. (2004) showed that sub-surface water flows and the resulted accumulation of sodium in clayey soils has great impact on rill and gully erosion processes and the associated formation of sub-surface pipes. Most works in the literature discuss sub-surface solutes transport due to rain water infiltration and leaching processes (e.g., Magaritz et al., 1988; Cantón et al., 2001; Faulkner et al., 2004) and ground water flows (e.g., Salama et al., 1999; Lamb et al., 2006; Fox and Wilson, 2010; Nachshon et al., 2014), with groundwater seepage playing an important role in soil salinization along slopes and stream channel banks (e.g., Matheson, 1968; Peck, 1978; Lamb et al., 2006).

Groundwater seepage is defined as water that emerges from rock or sediment, and seepage weathering is accordingly defined as the weathering processes facilitated by the seepage (Dunne, 1990; Lamb et al., 2006). In unconsolidated sediments, seepage erosion can occur without seepage weathering if the discharge of the seepage water is sufficient to detach and transport the sediments. However, in consolidated materials such as rocks, cohesive sands or cemented soils, seepage weathering is needed to reduce the material's cohesion before seepage erosion can occur (Dunne, 1990; Lamb et al., 2006). Seepage weathering breaks the parent material or reduces its resistivity for erosion due to the impact of seeping water on soil chemical and physical properties. Seepage weathering mechanisms may include chemical dissolution, frost growth, solutes accumulation and salt precipitation. The latter is a process by which evaporation preferentially removes the water while leaving the solutes, resulting in a soil layer with high erosivity. The major seepage-weathering processes discussed in the literature with respect to salinity and sodicity are: (1) weathering of alkaline and clayey soils, since 2:1 clay minerals (for example smectite) are sensitive to the presence of sodium in the exchange complex, which causes them to swell and disperse (deflocculate) (Salama et al., 1999; Vandekerckhove et al., 2000; Faulkner et al., 2000, 2004; Pulice et al., 2012), and (2) mechanical breaking of the soil matrix due to salt crystallization within pores that generates pressure against the pore walls ( Wellman and Wilson, 1965, 1968; Cantón et al., 2001; Lamb et al., 2006, 2008). The location of seepage and associated salinization and weathering processes is greatly affected by the soil hydraulic properties and conditions (e.g., Faulkner et al., 2004; Wilson et al., 2012), therefore it is crucial to understand the subsurface hydrological processes in order to predict and cope with soil salinization and erosion processes.

While groundwater seepage-erosion processes and the formation of bank undercuts have been explored for humid environments in both

http://dx.doi.org/10.1016/j.geomorph.2016.03.011
0169-555X/

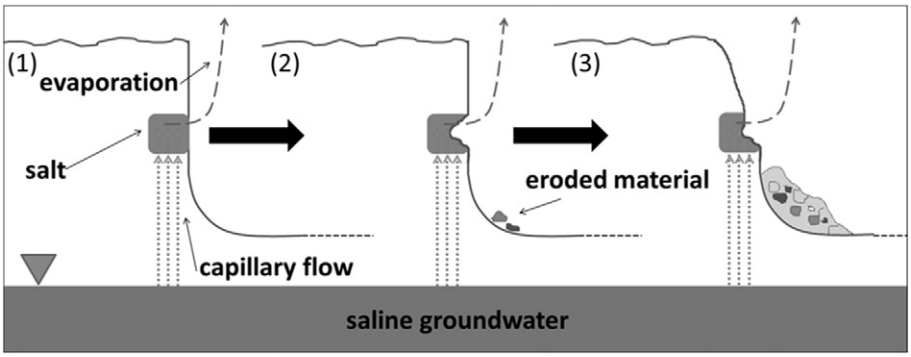


**Fig. 1.** Conceptual model of salt weathering at a gully bank. Thick black arrows and 1, 2, and 3 indicate temporal progress. At time 1, salt accumulates at the bank; at time 2, weathering starts at the site of salt accumulation and at time 3, the wall above the weathering height collapses. The thickness of the salt-accumulation band in the figure is not to scale as thickness and height may vary, depending upon the hydrogeological conditions.

the laboratory (Faulkner et al., 2004; Fox et al., 2007a; Wilson et al., 2007, 2012) and the field (Poesen et al., 2003; Fox et al., 2007b; Lamb et al., 2007, 2008), very limited work has been done on these processes in arid environments. In this manuscript, a novel conceptual model is presented to explain the formation of cavities along dry stream channels and gully banks in arid environments with limited subsurface seepage. The proposed concept is discussed in light of field observations, experimental results and a physically-based model.

## 2. Conceptual model

It is proposed that in arid environments, salt weathering may occur along gully and stream channel banks due to capillary rise of saline solutions from shallow and saline ground water (where it persists). It is suggested that capillary rise of the saline ground water along the vertical banks will lead to salt accumulation in a relatively narrow layer at the upper part of the capillary fringe and consequently, salt weathering will take place in that region. This will be followed by soil erosion due to fluvial and alluvial processes which will lead to the formation of pipe-shaped cavities along the gully and stream channel banks (Fig. 1). Hereon these cavities will be referred to as pipes, even though in the literature pipes are considered as cavities that form at the subsurface in parallel to the slope, due to underground water flows (Dunne, 1990; Faulkner, 2006; Fox and Wilson, 2010).

Intuitively, one would expect solutes to accumulate all along the vertical flow path at the banks, up to the upper boundary of the capillary fringe. This is because evaporation acts homogeneously over the vertical soil–atmosphere interface. Explaining the salt accumulation as a narrow layer at elevated levels (Fig. 1) is a key element of the proposed conceptual model. It is well known that salt precipitates out of a solution only when solutes concentration reaches saturation and that in natural environments, evaporation is a major cause of increased solutes concentration (Hillel, 2004). It is proposed here that for the case of saline water that flows upwards from a water table by capillarity through porous media, with a vertical face exposed to the atmosphere, liquid water fluxes in the matrix can be much faster in comparison to evaporative fluxes over the matrix–atmosphere interface, for most parts of the flow path. Consequently, the impact of evaporation on the solution concentration will be minor, as the upward-flowing water will continuously wash out the pore water. It is only at the top of the capillary fringe, where vertical liquid water fluxes are close to zero, that the evaporative water flux will be high enough, in comparison to the vertical liquid flux, to result in salt precipitation due to an increase in pore solution concentration. In Nachshon and Weisbrod (2015), a computation of liquid transport in porous media and vapour transport from the media to the atmosphere was performed for sand, sandy loam, and clay soils. It was shown that the liquid transport rates can be a few orders of magnitude higher than the evaporative diffusive vapour transport rates, down to matric potentials of approximately −0.35, −2, and −10 m (of $H_2O$) for sand, sandy loam and clay soils, respectively. The numerical model in the presented work will enable examination and comparison of the liquid and vapour transport rates in the system.

## 3. Numerical model

To simulate water and solute transport from the water table to the atmosphere due to evaporation along a vertical wall, a 1D model was constructed to solve the advection–dispersion and vapour diffusion equations numerically. Fig. 2 provides a conceptual presentation of the modelled domain and transport mechanisms.

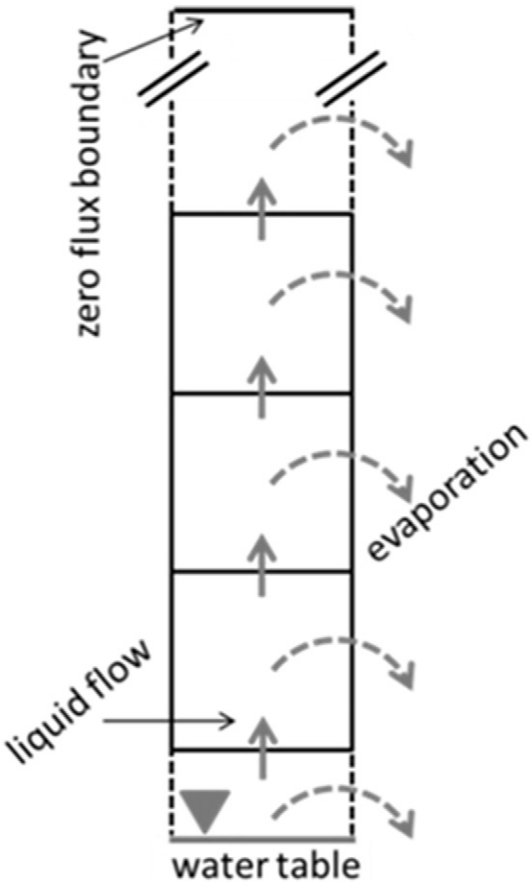


**Fig. 2.** Schematic diagram of the numerical model concept. Liquid fluxes between any two adjacent nodes depend upon hydraulic gradients and conductivity; evaporation from each node towards atmosphere was calculated based upon vapour pressure gradients and diffusivity.

The length of the modelled domain was 0.6 m, with height increments of 0.01 m. The lower boundary was determined as a Dirichlet boundary condition with a constant pressure head equal to zero (water table) and a solution concentration of 170 g of salt per 1000 g of water. The upper boundary condition was determined as zero-flux for both liquid and solutes. A sink term for water (with no solutes) was considered for each node and it was determined by calculation of the evaporative demand. The hydrostatic equilibrium state was set as the initial pressure head condition along the domain. This means that the matric potential of each node is equal to the negative of its height above the water table level, i.e., the lower boundary, in meters. Initial salt concentration along the domain was equal to the salt concentration at the lower boundary. These initial conditions are in accordance with the experimental work described in Sections 4.3 and 4.4. For liquid water transport, the Richards' equation was solved numerically:

$$\frac{\partial\psi}{\partial t}=\frac{1}{C(\psi)}\left(\frac{\partial}{\partial z}\left\{-K(\psi)\left[\frac{\partial\psi}{\partial z}+1\right]\right\}-S\right) \tag{1}$$

where $\psi$[m of $H_2O$] is the matric potential, $t$ is the time [s], $C(\psi)$ [1/m] is the specific capacity as a function of $\psi$, $z$ [m] is the vertical length, and $K(\psi)$ [m/s] is the hydraulic conductivity of the matrix as a function of $\psi$. $S$ [1/s] is the water loss to evaporation, which following Bohrer et al. (2005) and Mayer et al. (2012), is considered as a sink term governed by water vapour diffusion to the atmosphere. $K(\psi)$ is described by the Van Genuchten (1980) and Mualem (1976) models:

$$K(\psi)=K_S S_e^{0.5}\left[1-\left(1-S_e^{1/m}\right)^m\right]^2 \tag{2}$$

where $S_e$ is the effective saturation with respect to water:

$$S_e=\frac{\theta-\theta_r}{\theta_s-\theta_r} \tag{3}$$

$K_s$ [m/s] is the matrix hydraulic conductivity at saturation, $n$[−] and $\alpha$ [1/m] are the van Genuchten parameters (Table 1), $m=1-(1/n)$ [−] and $\theta$ is water content [−] with 'r' and 's' indicating residual and saturated water contents, respectively.

The sink term, $S$, which describes water loss from each node to evaporation (Fig. 2), is determined by the rate of vapour transport from the matrix to the atmosphere, $J$ [m/s]:

$$S=\frac{JA}{V} \tag{4}$$

where $A$ [$m^2$] is the surface area through which evaporation is taking place and $V$ [$m^3$] is the volume from which the water is being evaporated. $J$ is governed by the vapour concentration difference $\partial C_v$ [$kg/m^3$] over a boundary layer between matrix and atmospheric air $\partial x_v$ [m], the vapour diffusion coefficient, $D_v$ [$m^2/s$] (equal to ~$2.7\times10^{-5}$ in free air at ~25 °C (Cussler, 1997)), and water density, $\rho_w$ [1000 $kg/m^3$]:

$$J=-D_v\frac{\partial C_v}{\partial x_v}/\rho_w. \tag{5}$$

Matric potential and vapour concentration in unsaturated pores are coupled by Kelvin's law (e.g., Ho and Webb, 2006; Veran-Tissoires and Prat, 2014):

$$P_v=P_{sat}\exp\left(\frac{\psi}{\rho_w RT}\right) \tag{6}$$

where $P_{sat}$ [Pa] is the water vapour pressure at saturation (~4200 Pa for water at 30 °C), $R$ is the gas constant of water (462 J/kg K), $T$ [K] is the absolute temperature and $P_v$ is the vapour pressure in the pores, which is correlated to the vapour concentration (e.g., Ho and Webb, 2006) by:

$$C_v=\frac{P_v}{RT}. \tag{7}$$

In the model, it was assumed that atmospheric air has 10% relative humidity (equivalent to a water vapour concentration of 0.003 $kg/m^3$), therefore:

$$\partial C_v=0.003-C_v \tag{8}$$

$\partial x_v$ was considered to be $1\times10^{-3}$ m which is a reasonable boundary layer thickness for evaporative processes.

Changes in solute concentration, $\partial C_s$ [$kg/m^3$], with time along the simulated profile are formulated by the advection–dispersion equation which describes solute transport in porous media (e.g., Leij and van Genuchten, 2002):

$$\frac{\partial C_s}{\partial t}=D_e\frac{\partial^2 C_s}{\partial z^2}-v\frac{\partial C_s}{\partial z} \tag{9}$$

where $D_e$ [$m^2/s$] is the effective diffusion coefficient of the solutes and $v$ [m/s] is the liquid flow velocity which is equal to $q/\theta$, where $q$ is the liquid water flux between any two adjacent nodes in the model and is equal to:

$$q=-K(\psi)\left[\frac{\partial\psi}{\partial z}+1\right]. \tag{10}$$

$D_e$ is affected by water content and can be described by adopting the equation of Millington and Quirk (1961), as presented by Leij and van Genuchten (2002):

$$D_e=\frac{\theta^{7/3}}{\theta_s^2}D_0 \tag{11}$$

where $D_0$ [$m^2/s$] is the solute diffusion coefficient in free water. In the model, $D_0$ was taken as $2\times10^{-9}$ [$m^2/s$], which is a typical diffusion coefficient for ions in water. Eqs. (1) and (9) were solved numerically, and integrated in time using the ordinary differential equation solver, ODE15s, available in MATLAB.

## 4. Materials and methods

### 4.1. Field site

The field site is at the Gerar wash basin in the northern Negev Desert, Israel, in the section between Shoval and Tidhar (Fig. 3). The regional climate is semi-arid with an average evaporation of ~2000 mm/year

**Table 1**
Fine and coarse sand hydraulic properties.

| | $\alpha$[1/m] | $n$ [−] | $m$ [−] | $\theta_r$($m^3/m^3$) | $\theta_s$($m^3/m^3$) | $K_s$ [m/s] |
|---|---|---|---|---|---|---|
| Coarse sand | 7.9 | 3.9 | 0.744 | 0.07 | 0.36 | $1.6\times10^{-4}\pm2.11\times10^{-5}$ |
| Fine sand | 1.7 | 6.4 | 0.844 | 0.07 | 0.36 | $5.27\times10^{-5}\pm8.43\times10^{-6}$ |

and low precipitation, in the order of 200 mm/year (data from the Israeli Meteorological Service). The area lithology consists of an ~15 m-thick layer of loess soil overlying a massive chalk layer from the Avdat group (Yaalon and Dan, 1974; Weinberger and Rosenthal, 1994), which is not exposed at the examined region. The loess soil of the north-western Negev typically consists of 30% sand, 40% silt and 30% clay (Ginzburg and Yaalon, 1963; Gvirtzman et al., 2008). However, in the area of the research the loess contains a higher fraction of sand, in the order of 60%, as measured by Zaady et al. (2007). In general, the sediment profile includes a sequence of alternating silty-sand and sandy-clay loess units, with different compositions of sand, silt and clay. These layers are highly variable in width and lateral extent. Within the loess profile, several calcic horizons with typical thickness in the order of 1–1.5 m were found at various depths (e.g., Magaritz et al., 1988; Melson and Van Beek, 1992), representing wet periods during which salts that accumulated during previous drier periods leached and washed downward (Gvirtzman et al., 2008).

Most of the area is cultivated, primarily for wheat, corn and other annual crops. The main stream channel and its immediate surroundings are not cultivated and are partially covered by natural vegetation, with densities that vary with water availability. The entire basin overlies a shallow saline aquifer where, for topographical heights lower than 150 m (above sea level), the aquifer is exposed in the main stream channel (Fig. 3). The eastern parts of the region have a higher topographical elevation with greater distances between ground surface and the water table. For instance, on the east side of the research area, close to Shoval, ground surface elevation is about 200 m above sea level and groundwater level is at ~15 m depth as measured in an ancient well (Fig. 3). The most eastern point at which groundwater is exposed is indicated in Fig. 3. The main stream channel bank heights vary between 1 and 10 m and depths of gullies in the area are in the order of 1–4 m, depending on topography.

### 4.2. Field measurements

Visual observations along the stream channel and gullies in the area indicated the occurrence of erosion processes that lead to the formation of pipe-like cavities along the banks, as well as sapping processes. The eroded channels were photographed and their location was marked on the map. In two randomly selected representative locations (gullies 2 and 3 in Fig. 3), 100 $cm^3$ undisturbed soil samples were collected along the gully banks from top to bottom. The samples were sealed in plastic bags and analysed in the laboratory for salt concentration by the 1:1 saturated-paste extraction method (Corwin and Lesch, 2003; Zhang et al., 2005). In addition, three samples from each profile, from its top, centre and from within the pipe, with two repetitions for each height were analysed for water content, bulk density and texture. Water content (gravimetric) was measured by weighing the soil samples before and after drying of the samples at 105 °C for 48 h; bulk density was calculated by dividing mass of the dry samples by their volume; and texture analysis was done by the hydrometer method (Huluka and Miller, 2014).

At the locations of soil sampling, groundwater levels are approximately 1 m below gully bottoms. Groundwater samples were collected from the ancient well (Fig. 3) and at the Gerar Wash channel, where ground water is exposed (Fig. 3). Electrical conductivities (EC) of ground water and of the solutions extracted from the soil samples were measured by a standard EC meter (86505-pH/ORP/Cond./TDS/Salinity, AZ Instruments, Taiwan). At the examined banks in gullies 2 and 3, soil resistance for shearing was determined with a Torvane device (H-4212 1, Humbolt Manufacturing Company, IL, USA). The Torvane device was pressed against flat surfaces along the gully banks, close to the locations of soil sampling and the torque required to shear the soil was measured. Five repetitions were conducted for each height.

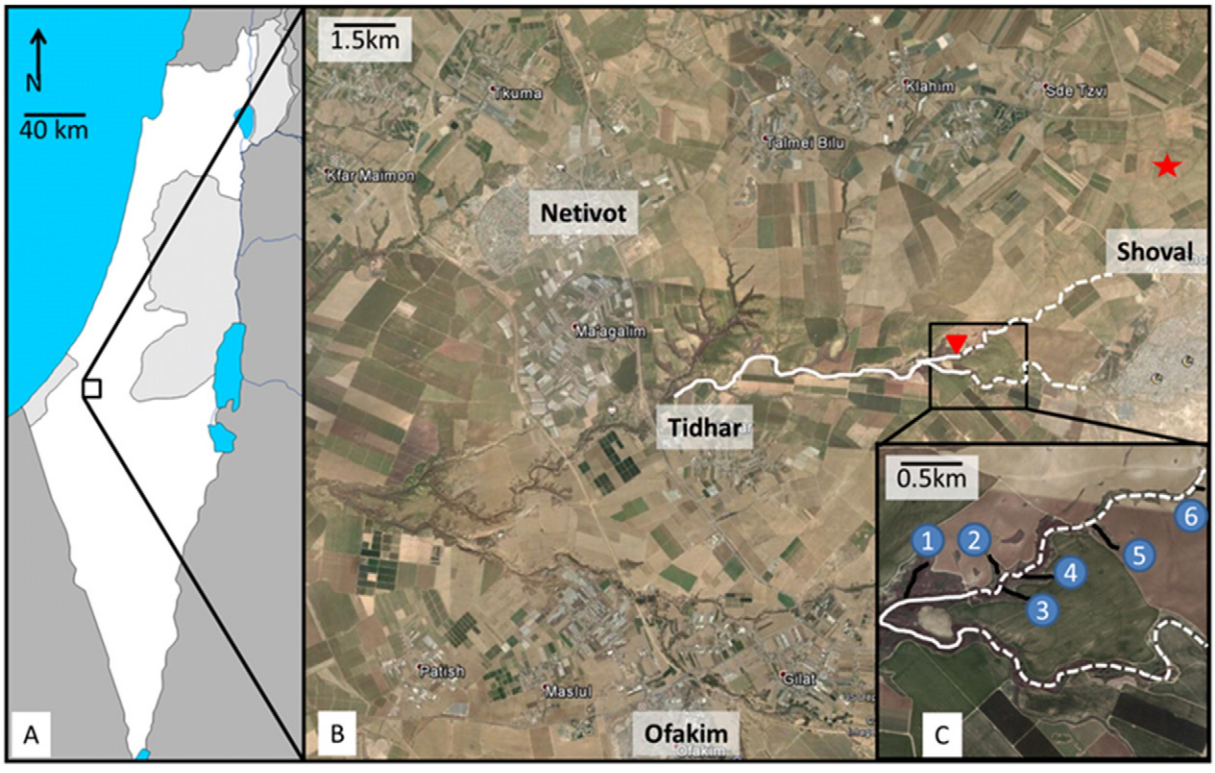


**Fig. 3.** Research site. (A) Israel and the northern Negev region. (B) Gerar basin with the main stream channel running between Kibbutz Shoval (Shoval) and Tidhar. (C) Enlargement of the research site. Solid white line indicates the wet stream channel where the aquifer is exposed, and dashed white lines indicate the dry stream channel. Black lines emphasize the main gullies at the site, numbered in circles. Star and triangle indicate locations of an ancient well that reaches the ground water at a depth of 15 m and the eastern-most location of groundwater exposure in the stream channel, respectively.

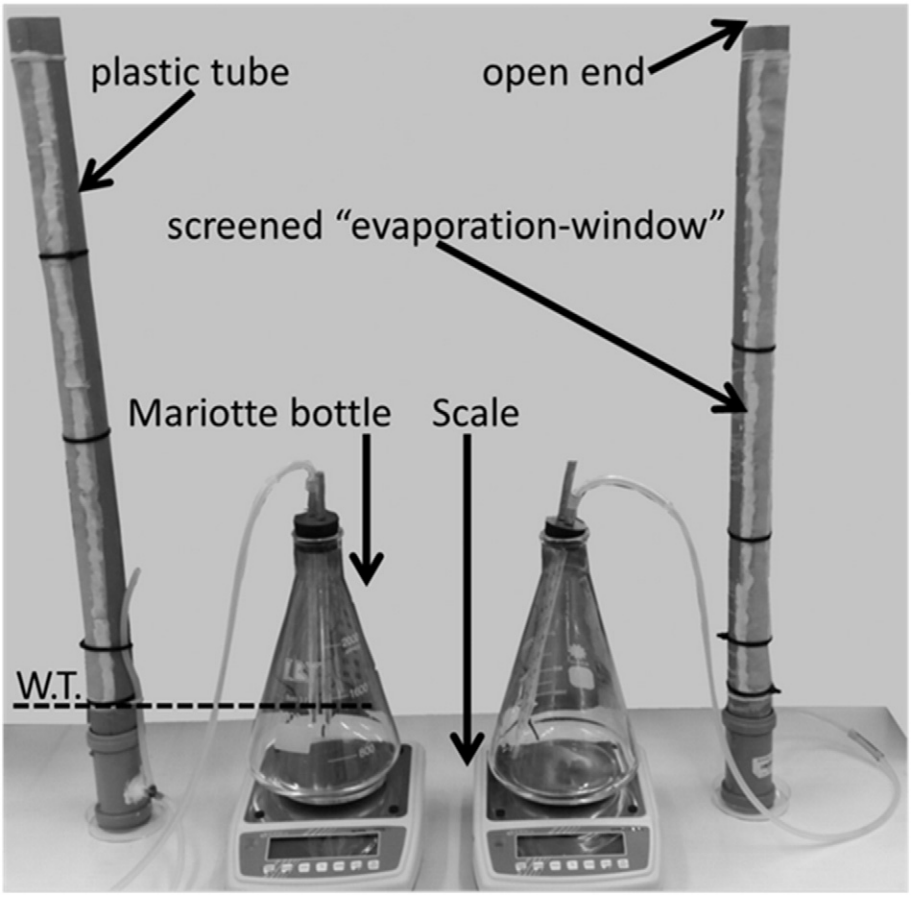


**Fig. 4.** Experimental set-up with the “evaporation windows” in plastic tubes that mimic the banks through which evaporation occurs. Each tube is connected to a Mariotte bottle that supplies saline solution, under constant pressure head.

### 4.3. Experimental set-up

Following the field observations of piping erosion at very specific heights (as will be presented in Section 5.1), the laboratory study and the numerical model were aimed at identifying the location of salt accumulation and understanding why it accumulates there. For this purpose, a 70 cm-long plastic tube, 5.08 cm in diameter, was used. The tube was sealed for liquid transport at its bottom and perimeter, apart from a slot, ~2.5 cm in width and 60 cm in length, which was cut along the tube; 2 and 8 cm of the tube at its top and bottom, respectively, were not slit, to maintain tube strength. In addition, the tube bottom was connected to a Mariotte bottle to maintain a constant water table at the lower boundary of the slot. The slot was covered by a fine fabric mesh (opening of 200 μm) so that the tube could be filled with sand. The slot was designed to function as an "evaporation window"

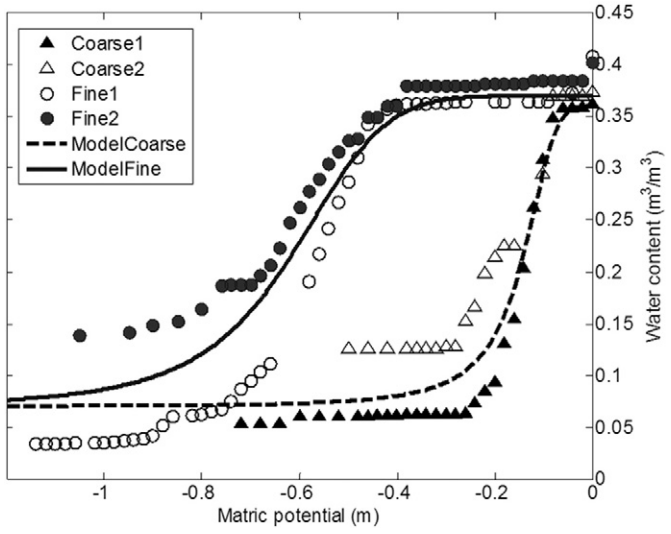


**Fig. 5.** Water-retention curves for the fine and coarse sands with two repetitions for each sand size. Solid and dashed curves are the models fitted to the measurements that were used to determine VG parameters.

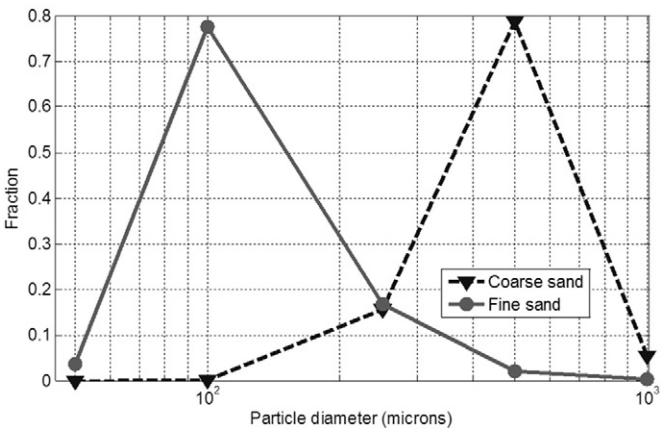


**Fig. 6.** Grain-size distributions of fine and coarse sands.

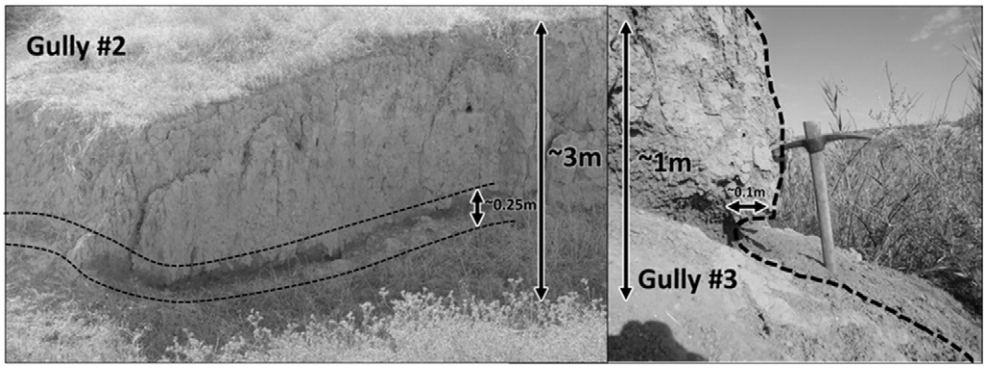


**Fig. 7.** Typical pipe erosion along gully banks at the field site. Gullies 2 and 3 are numbered according to the gully locations presented in Fig. 3. Dashed black lines mark the eroded pipes.

and mimic the vertical gully walls that are exposed to atmosphere and evaporation. The Mariotte bottle was filled with NaCl solution at a relatively high mass concentration of 15% (170 g/L) in order to accelerate the experiment and salt precipitation. The Mariotte bottle was placed on a scale (Precision Balance PFB, Kern, Germany, 0.001 mg accuracy) to measure water loss from the tube to evaporation. Fig. 4 presents the experimental setup.

### 4.4. Experimental procedure

Two types of air dried and salt free quartz sands, fine and coarse, were used in the experiment. The sands originated from a quarry in the central Negev, Israel. Tubes were tightly filled with each sand type, by pouring the sand through a nozzle from the upper part of the tube, while gently shaking the tube to ensure tight packing. The Mariotte bottle containing the saline solution was then connected to the bottom of the plastic tube, below the "evaporation window" and water level was set to ~1 cm below the lower boundary of this "window" by adjusting the tube height above the Mariotte bottle. Free flowing water was allowed to saturate the tube bottom and replenish the capillary flow of the solution upward. Changes in the Mariotte bottle's weight were monitored and after ~3 h of saturation, no significant changes were observed. It was assumed that the system is in a steady state and that any further change in the mass of the Mariotte bottle would be due to evaporation. At this point, the experiment was initiated. The tubes were left to evaporate for three days in the laboratory, while connected to the Mariotte bottles, at an ambient air temperature of ~25 °C. After three days of evaporation, the Mariotte bottles were disconnected and the fabric mesh was carefully peeled off. Sand samples were taken along the sand column from the lower boundary of the "evaporation window" up to 5 cm above the uppermost location of the capillary fringe, at 1 cm intervals. The sand samples were examined for (mass) water content by measuring their wet weight and oven-dry weight after 48 h at 105 °C at 0.001 mg accuracy. Following the water content analysis, 10 g of sand was taken from each dry sample and salinity was measured by the 1:1 saturated paste extraction method.

Preliminary tests were conducted to characterize the two sand types with respect to hydraulic conductivity by the Darcy experiment over a 10 cm length tube with hydraulic gradient of 7 cm of $H_2O$ (Radcliffe and Rasmussen, 2002; Nachshon and Weisbrod, 2015); Van Genuchten (VG) parameters and porosity were determined by the pressure flow cell technique (Or and Wraith, 2002); and texture by shaking the sand through a shaking sieve system for 5 h (Skopp, 2002). Fig. 5 presents the measured water retention curves produced by the pressure flow cell method and the fitted models that were used to compute the VG parameters (van Genuchten, 1980). Variations in water retention curves for the same sand, especially at the higher matric potentials could be related to differences in the thermal conditions of the laboratory as the experiments were not conducted simultaneously (Nimmo and Miller, 1986), or due to other uncontrolled parameters such as differences in soil packing. Nevertheless, the curves show a good agreement in respect to the air entry pressure values of the two sands, which is the most

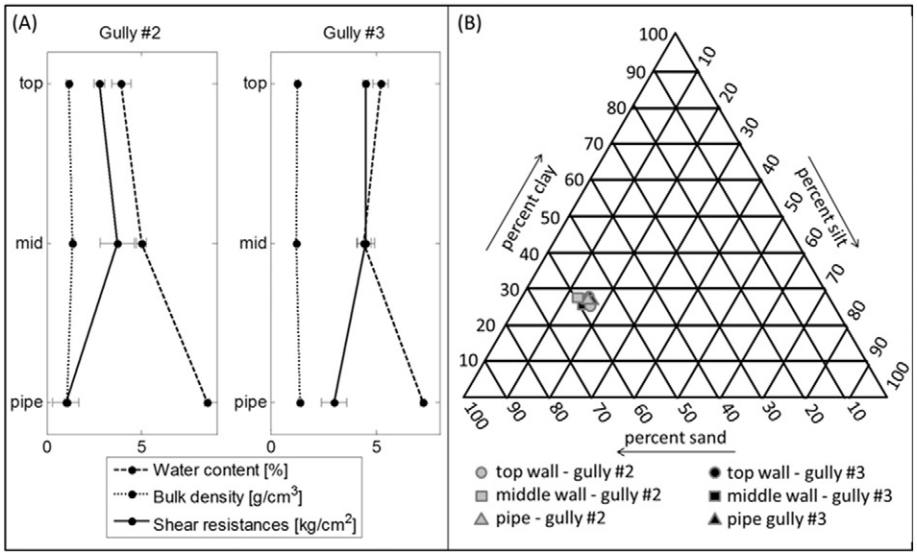


**Fig. 8.** (A) Soil physical properties along banks of gullies 2 and 3. 'top', 'mid' and 'pipe' indicate the location of sampling from top of the profile, from its centre (half way down towards the pipe), and from within the pipe. (B) Soil texture from gullies 2 and 3, which is defined as 'sandy clay loam'.

crucial parameter to estimate the height of capillary fringe. Fig. 6 presents the two sands' grain-size distributions. Darcy experiments indicated the hydraulic conductivity at saturation ($K_S$) for the coarse and fine sands, respectively, as summarized in Table 1.

## 5. Results and discussion

### 5.1. Field results

As already noted, at the research field site, similar to many other locations in the region, the formation of cavities along gully and stream channel banks is a common sight. The cavities are of various lengths and are located horizontally along the banks, approximately 1 m above the stream channels' and gullies' lower surfaces. The cavities have a pipe shape with height and depth of approximately 10–20 cm (Fig. 7).

Measured water contents in the soil samples taken from the inner parts of the cavities in gullies 2 and 3 were in the order of 10%, whereas in the upper parts of the profiles, above the pipes, water contents were in the order of 4%. Bulk densities were relatively uniform with averaged values of $1.23 \pm 0.12$ g/cm$^3$. Soil resistance to shear stress measured by the Torvane device was notably different between the bank soils above the pipes and within the pipes, with averaged values of $3.68 \pm 0.90$ kg/cm$^2$ and $1.66 \pm 1.25$ kg/cm$^2$, respectively. Soil texture along bank profiles and within the pipes was highly similar between all samples with averaged soil composition of 57.5% sand, 14.5% silt, and 28% clay. Fig. 8 summarizes the measured physical properties of the soil profiles along the banks of gullies 2 and 3. In the pipe-like cavities, salt crystals were visually observed (Fig. 9A) and EC analysis of soil samples taken from the two vertical profiles at gullies 2 and 3 indicated preferential accumulation of salts within the cavities (Fig. 9B, C).

Ground water samples from the ancient well and the Gerar wash channel (triangle and star symbols in Fig. 3) were saline with measured EC values of 11.58 and 13.29 dS/m, respectively. Based on the locations of gullies 2 and 3 and the elevation of the exposed ground water at the Gerar wash (Fig. 3), it is estimated that the water table below these gullies is at a depth of 1–2 m. In a few locations in these gullies the soil at ground surface was moist, indicating active capillary movement of water from the ground water upward (no rain events had been recorded at the site for several months before the measurements). Gvirtzman et al. (2008) reported an air entry pressure for loess in the order of 0.5–1 m and hydraulic conductivity in the order of $1.5 \times 10^{-5}$ m/s at a matric potential of −1 to −1.5 m, depending on the loess texture and clay content. These values support the field observations as they indicate that the capillary fringe in loess soils may rise up to a height of ~1.5 m. Since ground water at the site is saline, at least theoretically, it is reasonable to assume that ground water may flow upward by capillarity and salt crystallization may occur along gullies and stream channel banks, where evaporation is taking place. Moreover, the uniform texture and bulk density of the soil profiles, together with the low precipitation rates in the region strengthen the assumption that the source of moisture and salinity in the pipes is not from downward infiltration of rain or lateral flow of perched groundwater, which is the common explanation for seepage weathering and erosion (Faulkner et al., 2004; Fox et al., 2007b; Lamb et al., 2008; Wilson et al., 2012).

The field measurements support the proposed conceptual model (Fig. 1) as they show that soil erosion and pipe formation are associated with salt accumulation and crystallization, and indicate that the origin

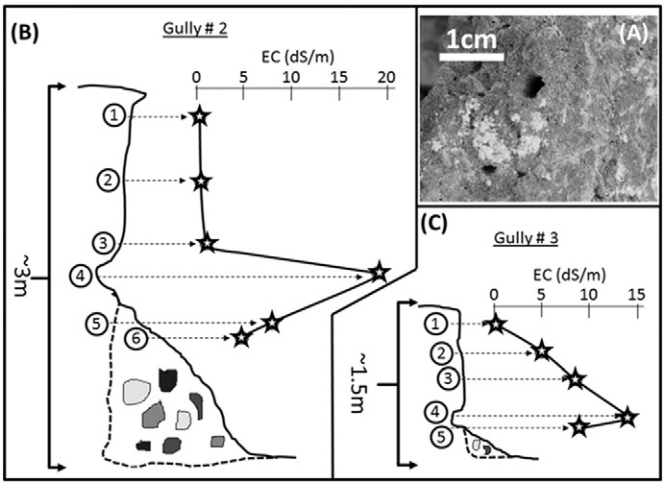


**Fig. 9.** (A) Salt crystals (white cluster) as observed in the pipe cavities. (B) and (C) Schematic drawings of vertical profiles along the randomly selected walls in gullies 2 and 3, respectively. Numbers indicate the locations of soil sampling. Stars and black curves represent the EC readings from the saturated-paste extractions. Irregular black and gray shapes represent the eroded material at the gully bottom. Dashed lines indicate the approximate locations of the original wall and gully base which are hidden by the eroded material.

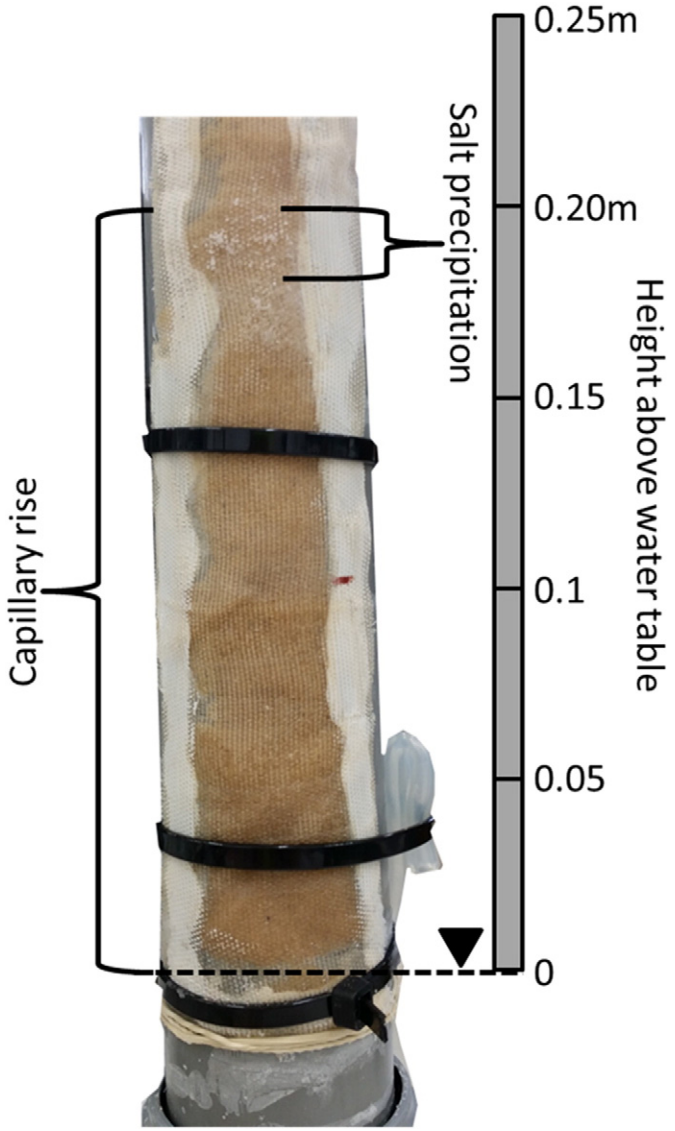


**Fig. 10.** Salt accumulation at the upper part of the capillary fringe, for the coarse sand column. The salt crystals are the white crumbles designated by 'Salt precipitation '. No other locations of salt precipitation were observed at the "evaporation window". Dashed line and black triangle indicate the height of water table level which was maintained by the Mariotte bottle.

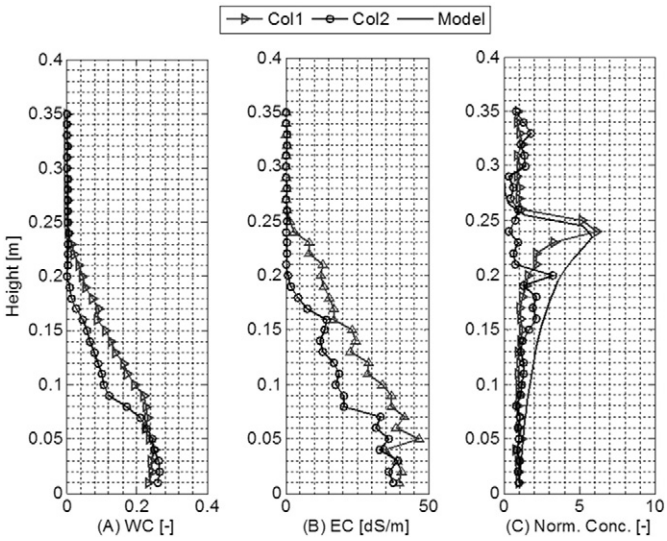


**Fig. 11.** Experimental and model results for the coarse sand columns ('Col1' and 'Col2' are repetitions). (A) Gravimetric water content. (B) EC of extracted water. (C) Normalized salt concentration.

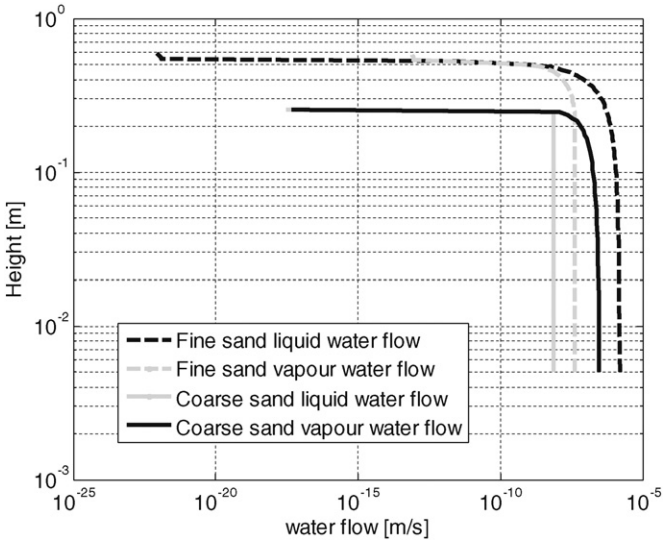


**Fig. 13.** Simulated water (liquid and vapour) flows.

of porewater and salts in the pipes is capillary rise of saline water from the shallow saline ground water. Nevertheless, the field observations cannot explain a key element of the conceptual model which is the salt accumulation in a narrow layer rather than over the entire height of capillary rise along the bank-atmosphere interface. In the following sections the laboratory experiments will be presented to show that capillary rise along a vertical wall can lead to salt accumulation over a narrow layer, even though evaporation is acting over the entire vertical wall.

### 5.2. Laboratory experiments and model results

After two days of evaporation through the "evaporation windows" of the sand columns, salt precipitation was visually observed in layers ~2 cm thick at the upper parts of the capillary fringe, both for the coarse (Fig. 10) and fine sand columns. Water content and salinity were measured along the fine and coarse sand columns after 3 days of evaporation. Figs. 11A and 12A present the measured gravimetric water content for the coarse and fine sands, respectively. It is seen that capillary rise is in the order of 0.2 and 0.4 m for the coarse and fine sands, respectively. These differences are a result of the differences in water retention properties between the two sands. Figs. 11B and 12B present the measured EC for the water extractions from the (1:1) saturated pastes for the coarse and fine sands, respectively. Figs. 11C and 12C present the normalized calculated salt concentration along the sand profiles for the coarse and fine sands, respectively. The normalized salt concentration was calculated by dividing the measured EC by the measured water content at each measurement point and dividing this value by the bottom value, at the lowest part of the "evaporation window", which reflects the source water concentration. In practice, this method provides the amount of salt accumulated in the soil profile relative to the original salt concentration in the feeding solution. Normalizing salt concentration is needed in order to observe the location of salt accumulation along the tubes. Because the feeding solution contained a high concentration of NaCl, high EC values were found in the lower parts of the columns that were fully saturated in respect to water when analysed by the saturated paste method, which cannot differentiate between salts that are already precipitated and dissolved salts in pore water. Figs. 11C and 12C also present the numerical model results of pore water salt concentrations normalized relative to the feeding solution concentration, after 3 days of evaporation. Cumulative evaporation from the tubes by the end of the experiment was in the order of 15 g and 50 g for the coarse and fine sands, respectively.

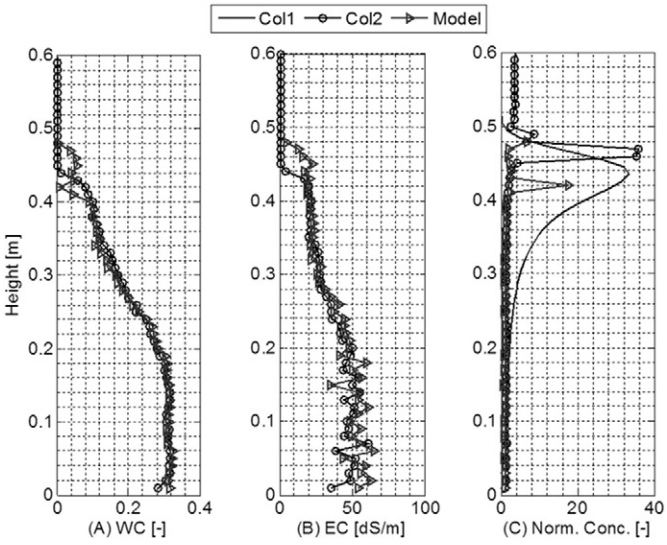


**Fig. 12.** Experimental and model results for the fine sand columns ('Col1' and 'Col2' are repetitions). (A) Gravimetric water content. (B) EC of extracted water. (C) Normalized salt concentration.

Maximal salt concentrations were measured in narrow layers several cm thick, at the upper boundary of the capillary rise (Figs. 10, 11, 12). At lower heights of the columns, even though the saline solution was available and exposed to evaporation, no increase in salt concentration was observed. The numerical model showed similar trends and a good fit to the experimental measurements. However, a good fit of the height of the concentration peak was achieved only after lowering $K_s$ of the modelled coarse and fine sands by one order and two orders of magnitude, respectively; for higher $K_s$ values, the model predicted salt accumulation a few centimetres above the height of the measured peak concentration. Fig. 13 presents the calculated liquid and vapour water fluxes along the soil profile at the end of day 3. For most of the profile, liquid water flow by capillarity was greater than the evaporation flux. Only at the top of the capillary fringe, where hydraulic conductivity and liquid fluxes tend to zero, was the evaporative demand high enough

to result in significant removal of the water that enabled an increase in the pore water salt concentration. Therefore, salt accumulated at the upper boundary of the capillary fringe and not all along the vertical wall, even though evaporation was occurring there as well.

## 6. Conclusions

A new conceptual model was proposed to explain the formation of pipe-like cavities in gully and dry stream channel banks in arid environments. Field observations and laboratory experiments showed that processes similar to seepage weathering are not limited to moist environments and they may occur also in arid regions, under unsaturated conditions. In contrast to the conventional explanation for salt weathering of soil along vertical walls by (saturated) subsurface flow and water seepage along stream channels and gully banks, the proposed model suggests accumulation of salt at these locations by capillary flow of saline water from the ground water. It was shown that the high liquid water flow rate compared to the slow evaporation flux results in accumulation of the salts in a narrow band at the top of the capillary fringe. The field observations, experimental study, and physical-based model simulations all indicated the proposed conceptual model to be an important mechanism to explain erosion processes in dry environments where shallow ground water persists. More work is needed in the field to estimate the magnitude and impact of the proposed mechanism relative to other erosion processes. If the proposed erosion mechanism is found to be significant, then future actions should be considered in saline and dry environments to reduce the risk of soil erosion. For example, a good solution might be to lower groundwater levels by planting halophytic vegetation, thereby stabilizing the soil.

## Acknowledgement

The author wishes to thank ARO for funding the research and Ms. Hee-Rae Cho and Mr. Katzir Roee for their assistance with the experimental parts of the work.

## References

Bohrer, G., Mourad, H., Laursen, T.A., Drewry, D., Avissar, R., Poggi, D., Oren, R., Katul, G.G., 2005. Finite element tree crown hydrodynamics model (FETCH) using porous media flow within branching elements: a new representation of tree hydrodynamics. Water Resour. Res. 41. http://dx.doi.org/10.1029/2005WR004181 (W11404+).

Cantón, Y., Solé-Benet, A., Queralt, I., Pini, R., 2001. Weathering of a gypsum-calcareous mudstone under semi-arid environment at Tabernas, SE Spain: laboratory and field-based experimental approaches. Catena 44, 111–132. http://dx.doi.org/10.1016/S0341-8162(00)00153-3.

Corwin, D., Lesch, S., 2003. Application of soil electrical conductivity to precision agriculture. Agron. J. 95, 455–471.

Cussler, E.W., 1997. Diffusion: Mass Transfer in Fluid Systems. second ed Cambridge University Press.

Dunne, T., 1990. Hydrology, mechanics, and geomorphic implications of erosion by subsurface flow. Groundw. Geomorphol. Role Subsurf. Water Earth-Surface Process. Landforms - Spec. Pap. Soc. Am. 252, pp. 1–28

Faulkner, H., 2006. Piping hazard on collapsible and dispersive soils in Europe. In: Boardman, J., Poesen, J. (Eds.), Soil Erosion in Europe. John Wiley and Sons, Ltd., Chichester, U.K., pp. 537–562.

Faulkner, H., Alexander, R., Teeuw, R., Zukowskyj, P., 2004. Variations in soil dispersivity across a gully head displaying shallow sub-surface pipes, and the role of shallow pipes in rill initiation. Earth Surf. Process. Landf. 29, 1143–1160. http://dx.doi.org/10.1002/esp.1109.

Faulkner, H., Spivey, D., Alexander, R., 2000. The role of some site geochemical processes in the development and stabilisation of three badland sites in Almería, Southern Spain. Geomorphology 35, 87–99.

Fox, G.A., Wilson, G.V., 2010. The role of subsurface flow in hillslope and stream bank erosion: a review. Soil Sci. Soc. Am. J. 74, 717. http://dx.doi.org/10.2136/sssaj2009.0319.

Fox, G.A., Chu-Agor, M.L. (Maria), Wilson, G.V., 2007a. Erosion of noncohesive sediment by ground water seepage: lysimeter experiments and stability modeling. Soil Sci. Soc. Am. J. 71, 1822. http://dx.doi.org/10.2136/sssaj2007.0090.

Fox, G.A., Wilson, G.V., Simon, A., Langendoen, E.J., Akay, O., Fuchs, J.W., 2007b. Measuring streambank erosion due to ground water seepage: correlation to bank pore water pressure, precipitation and stream stage. Earth Surf. Process. Landf. 33, 1558–1573.

Ginzburg, D., Yaalon, D.H., 1963. Petrology and origin of loess in the Beer Sheva basin. Isr. J. Earth Sci. 12, 68–70.

Gvirtzman, H., Shalev, E., Dahan, O., Hatzor, Y.H., 2008. Large-scale infiltration experiments into unsaturated stratified loess sediments: monitoring and modeling. J. Hydrol. 349, 214–229. http://dx.doi.org/10.1016/j.jhydrol.2007.11.002.

Hillel, D., 2004. Introduction to Environmental Soil Physics. Elsevier, New York.

Ho, C.K., Webb, S.W., 2006. Gas Transport in Porous Media. Springer Netherlands, Dordrecht.

Huluka, G., Miller, R., 2014. Particle size determination by hydrometer method. In: Moore, K.P. (Ed.), Sikora, F.J.Lexington, Soil Test Methods From the Southeastern United States, pp. 180–184

Lal, R., 2003. Soil erosion and the global carbon budget. Environ. Int. 29, 437–450. http://dx.doi.org/10.1016/S0160-4120(02)00192-7.

Lamb, M.P., Dietrich, W.E., Aciego, S.M., DePaolo, D.J., Manga, M., 2008. Formation of Box Canyon, Idaho, by megaflood: implications for seepage erosion on Earth and Mars. Science 320 (80-), 1067–1070.

Lamb, M.P., Howard, A.D., Dietrich, W.E., Perron, J.T., 2007. Formation of amphitheater-headed valleys by waterfall erosion aft er large scale slumping on Hawaii. Geol. Soc. Am. Bull. 119, 805–822.

Lamb, M.P., Howard, A.D., Johnson, J., Whipple, K.X., Dietrich, W.E., Perron, J.T., 2006. Can springs cut canyons into rock? J. Geophys. Res. E Planets 111, 1–18. http://dx.doi.org/10.1029/2005JE002663.

Leij, F.J., van Genuchten, M.T., 2002. Solute transport. In: Warrick, A.W. (Ed.), Soil Physics Companion. CRC Press, pp. 189–248.

Magaritz, M., Gvirtzman, H., Nadler, A., 1988. Salt accumulation in the loessial sequence in the Be'er Sheva Basin, Israel. Environ. Geol. Water Sci. 11, 27–33. http://dx.doi.org/10.1007/BF02587760.

Matheson, W.E., 1968. When salt takes over. J. Agric. South Aust. 71, 266–272.

Mayer, K.U., Amos, R.T., Molins, S., Gérard, F., 2012. In: Zhang, F., Yeh, G.-T., Parker, J.C. (Eds.), Reactive Transport Modeling in Variably Saturated Media with MIN3P: Basic Model Formulation and Model Enhancements. Bentham Science Publishers, Groundwater Reactive Transport Models, pp. 186–212.

Melson, W.G., Van Beek, G.W., 1992. Geology and the loessial soils, Tell Jemmeh, Israel. Geoarchaeology 7, 121–147.

Millington, R.J., Quirk, J.P., 1961. Permeability of porous solids. Trans. Faraday Soc. 57, 1200–1207.

Mualem, Y., 1976. A new model of predicting hydraulic conductivity of unsaturated porous media. Water Resour. Res. 12, 513–522.

Nachshon, U., Weisbrod, N., 2015. Beyond the salt crust: on combined evaporation and subflorescent salt precipitation in porous media. Transp. Porous Media http://dx.doi.org/10.1007/s11242-015-0514-9.

Nachshon, U., Ireson, A., van der Kamp, G., Davies, S.R., Wheater, H.S., 2014. Impacts of climate variability on wetland salinization in the North American prairies. Hydrol. Earth Syst. Sci. 18, 1–14. http://dx.doi.org/10.5194/hess-18-1-2014.

Nimmo, J.R., Miller, E.E., 1986. The temperature dependence of isothermal moisture vs. potential characteristics of soils. Soil Sci. Soc. Am. J. 50, 1105. http://dx.doi.org/10.2136/sssaj1986.03615995005000050004x.

Or, D., Wraith, J.M., 2002. Soil water content and water potential relationships. In: Warrick, A.W. (Ed.), Soil physics companion. CRC Press, New York, pp. 49–84.

Peck, A.J., 1978. Salinization of non-irrigated soils and associated streams: a review. Aust. J. Soil Res. 16, 157–168. http://dx.doi.org/10.1071/SR9780157.

Poesen, J., Nachtergaele, J., Verstraeten, G., Valentin, C., 2003. Gully erosion and environmental change: importance and research needs. Catena 50, 91–133. http://dx.doi.org/10.1016/S0341-8162(02)00143-1.

Pulice, I., Cappadonia, C., Scarciglia, F., Robustelli, G., Conoscenti, C., De Rose, R., Rotigliano, E., Agnesi, V., 2012. Geomorphological, chemical and physical study of "calanchi" landforms in NW Sicily (southern Italy). Geomorphology 153-154, 219–231. http://dx.doi.org/10.1016/j.geomorph.2012.02.026.

Radcliffe, D.E., Rasmussen, T.C., 2002. Soil water movement. In: Warrick, A.W. (Ed.), Soil Physics Companion. CRC press, New York, pp. 65–126.

Salama, R.B., Otto, C.J., Fitzpatrick, R.W., 1999. Contributions of groundwater conditions to soil and water salinization. Hydrogeol. J. 7, 46–64. http://dx.doi.org/10.1007/s100400050179.

Skopp, J.M., 2002. Physical properties of primary particles. In: Warrick, A.W. (Ed.), Soil Physics Companion. CRC press, New York, pp. 1–16.

van Genuchten, M.T., 1980. A closed-form equation for predicting the hydraulic conductivity of unsaturated soils. Soil Sci. Soc. Am. J. 44, 892–898.

Vandekerckhove, L., Poesen, J., Oostwoud Wijdenes, D., Gyssels, G., Beuselinck, L., De Luna, E., 2000. Characteristics and controlling factors of bank gullies in two semi-arid mediterranean environments. Geomorphology 33, 37–58. http://dx.doi.org/10.1016/S0169-555X(99)00109-9.

Veran-Tissoires, S., Prat, M., 2014. Evaporation of a sodium chloride solution from a saturated porous medium with efflorescence formation. J. Fluid Mech. 749, 701–749. http://dx.doi.org/10.1017/jfm.2014.247.

Weinberger, G., Rosenthal, E., 1994. The fault pattern in the northern Negev and southern Coastal Plain of Israel and its hydrogeological implications for groundwater flow in the Judea Group aquifer. J. Hydrol. 155, 103–124.

Wellman, H.W., Wilson, A.T., 1965. Salt weathering, a neglected geological erosive agent in coastal and arid environments. Nature 205, 1097–1098.

Wellman, H.W., Wilson, A.T., 1968. Salt weathering or fretting. In: Fairbridge, R.W. (Ed.), The Encyclopedia of Geomorphology. Reinhold Book, New York City, N. Y., pp. 968–970.

Wilson, G.V., Nieber, J.L., Sidle, R.C., Fox, G.A., 2012. Internal Erosion During Soil Pipeflow: State of the Science for Experimental and Numerical Analysis. Trans. ASABE 56, 465–478. http://dx.doi.org/10.13031/2013.42667.

Wilson, G.V., Periketi, R.K., Fox, G.A., Dabney, S.M., Shields, F.D., Cullum, R.F., 2007. Soil properties controlling seepage erosion contributions to streambank failure. Earth Surf. Process. Landf. 32, 447–459.

Wilson, G.V., Rigby, J.R., Dabney, S.M., 2015. Soil pipe collapses in a loess pasture of Goodwin Creek watershed, Mississippi: role of soil properties and past land use. Earth Surf. Process. Landf. 1463. http://dx.doi.org/10.1002/esp.3727 (n/a–n/a).

Yaalon, D., Dan, J., 1974. Accumulation and distribution of loess-derived deposits in the semi-desert and desert fringe areas of Israel. Z. Geomorphol. Suppl. 91.

Zaady, E., Karnieli, A., Shachak, M., 2007. Applying a field spectroscopy technique for assessing successional trends of biological soil crusts in a semi-arid environment. J. Arid Environ. 70, 463–477. http://dx.doi.org/10.1016/j.jaridenv.2007.01.004.

Zhang, H., Schroder, J.L., Pittman, J.J., Wang, J.J., Payton, M.E., 2005. Soil salinity using saturated paste and 1:1 soil to water extracts. Soil Sci. Soc. Am. J. 69, 1146. http://dx.doi.org/10.2136/sssaj2004.0267.